

Effective field theory for triple-Q magnetic orders on a hexagonal lattice

Jin-Tao Jin¹ and Yi Zhou^{2,*}

¹*Department of Physics, The Hong Kong University of Science and Technology, Clear Water Bay, Kowloon 999077, Hong Kong, China*

²*Institute of Physics, Chinese Academy of Sciences, Beijing 100190, China*

We develop a comprehensive Ginzburg-Landau theory describing triple-Q magnetic orders on hexagonal lattices, focusing on $O(N)$ models with $N = 2$ and $N = 3$. Through systematic analysis of symmetry-allowed terms in the free energy, we establish complete phase diagrams governed by competing interaction parameters. Our theory reveals distinct magnetic configurations including single-Q, double-Q, and triple-Q states, each characterized by unique symmetry breaking patterns and collective excitations. The framework provides fundamental insights into complex magnetic orders recently observed in materials such as $\text{Na}_2\text{Co}_2\text{TeO}_6$, where the interplay between geometric frustration and multiple ordering vectors leads to exotic magnetic states. Our results establish clear connections between microscopic interactions, broken symmetries, and experimentally observable properties, offering a powerful tool for understanding and predicting novel magnetic phases in frustrated magnets.

Introduction — The Ginzburg-Landau (GL) theory serves as a cornerstone in understanding classical phase transitions and ordered states in condensed matter systems [1, 2]. Through systematic application of symmetry principles and order parameter expansions, the GL framework provides crucial insights into systems where competing interactions lead to complex phase diagrams and sophisticated ordering configurations.

In magnetic systems, the interplay between geometric frustration, spin-orbit coupling, and anisotropic exchange interactions gives rise to intricate multiple-Q magnetic structures that extend beyond conventional single-Q arrangements [3, 4]. These multiple-Q configurations are particularly significant in hexagonal lattices, where they can generate novel topological features and unusual transport phenomena [5, 6]. Recent investigations of neutron scattering and thermal transport have revealed detailed magnetic patterns in materials such as $\text{Na}_2\text{Co}_2\text{TeO}_6$ [7–10], as also indicated in the Kitaev candidate material $\alpha\text{-RuCl}_3$ [11–14]. Similar complex ordering patterns have been observed in $\text{Na}_3\text{Co}_2\text{SbO}_6$ [15, 16] and related compounds [17–19].

Of particular importance is the emergence of triple-Q states, which represent a distinct class of magnetic order stabilized by competition among different exchange interactions [20]. While both theoretical studies [21–24] and experimental observations [7, 8] have highlighted the significance of these states, a comprehensive theoretical framework capable of explaining their formation and stability remains an outstanding challenge.

In this study, we develop a comprehensive GL theory for triple-Q magnetic orders on a hexagonal lattice. We define three order parameters, $\Delta_{\mathbf{Q}_l}$ ($l = 1, 2, 3$), each corresponding to a pair of M points within the Brillouin zone, with each $\Delta_{\mathbf{Q}_l}$ representing an $O(N)$ multiplet. This approach provides sufficient generality to encompass a range of magnetic orders while remaining strictly governed by the inherent D_3 lattice symmetry [25–28].

Through detailed examination of system stability and various phases via GL free energy minimization, we focus particularly on the experimentally relevant cases of $N = 2$ and $N = 3$ [29, 30]. Our analysis yields comprehensive phase diagrams and clarifies the distinct configurations of order parameters under different conditions. Furthermore, we investigate collective excitations and symmetry breaking phenomena associated with different phases [31–36].

Our theoretical framework directly connects to recent advances in Kitaev candidate materials [37–39] and frustrated magnetic systems [40–42]. The results provide clear directions for interpreting new experimental data and establish a foundation for potential applications in spintronics and quantum information technology [43, 44].

Model and Symmetry — To construct an effective field theory for triple-Q magnetic orders on hexagonal lattices, we consider an $O(N)$ model with order parameters represented as N -dimensional vectors:

$$\Delta_{\mathbf{Q}_l} = (\Delta_{\mathbf{Q}_l}^1, \Delta_{\mathbf{Q}_l}^2, \dots, \Delta_{\mathbf{Q}_l}^N)^T,$$

where each component $\Delta_{\mathbf{Q}_l}^p$ is real. These order parameters correspond to the three M -points in the first Brillouin zone denoted by wave vectors: $\mathbf{Q}_1 = Q(0, 1)$, $\mathbf{Q}_2 = Q(-1/2, -1/2\sqrt{3})$, and $\mathbf{Q}_3 = Q(1/2, -1/2\sqrt{3})$, as illustrated in Fig. 1(a).

The symmetry constraints of our system include the D_3 point group of the hexagonal lattice [45] and the internal $O(N)$ rotational symmetry of the order parameters. Incorporating these symmetries, we express the Ginzburg-Landau free energy up to quartic order as [46]:

$$\begin{aligned} \mathcal{F}_{O(N)} = & \alpha \sum_{l=1}^3 |\Delta_{\mathbf{Q}_l}|^2 + \beta_1 \sum_{l=1}^3 |\Delta_{\mathbf{Q}_l}|^4 \\ & + \beta_2 \sum_{l < m} |\Delta_{\mathbf{Q}_l}|^2 |\Delta_{\mathbf{Q}_m}|^2 + \beta_3 \sum_{l < m} (\Delta_{\mathbf{Q}_l} \cdot \Delta_{\mathbf{Q}_m})^2, \end{aligned} \quad (1)$$

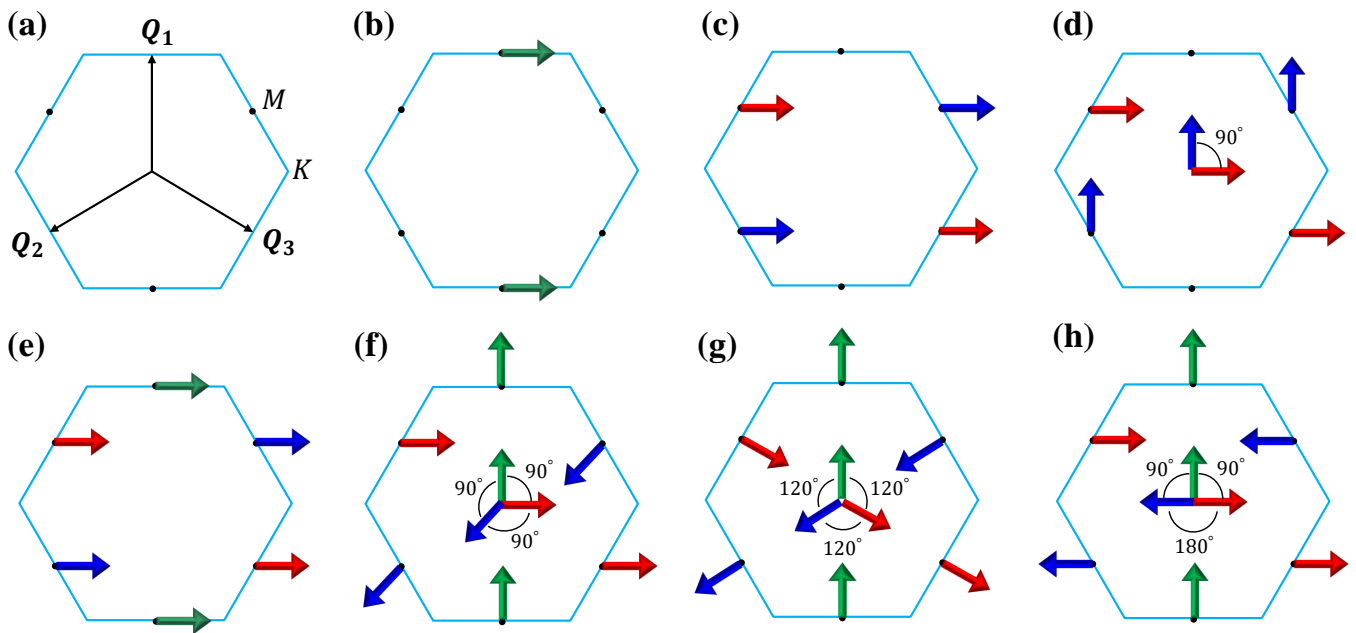


FIG. 1. (a) The triple Q-vectors Q_1 , Q_2 , and Q_3 are specified at the M points of the first Brillouin Zone on a hexagonal lattice. Note that $-Q_l$ is equivalent to Q_l at each M point, where $l = 1, 2, 3$. Multiple Q-vector magnetic configurations for $O(N)$ models include: single-Q (b) $I_{O(N=2,3)}$, double-Q (c) $II_{O(N=2,3)}^A$ and (d) $II_{O(N=2,3)}^B$, and triple-Q (e) $III_{O(N=2,3)}^A$ (collinear), (f) $III_{O(3)}^B$ (orthogonal), (g) $III_{O(2)}^C$ (120° coplanar), and (h) $III_{O(2)}^D$ (orthogonal-collinear) states. The vectors that are collinear at distinct Q_l in (c), (e) and (h) may align in parallel or opposite directions. The configuration in (f) has three mutually orthogonal vectors, which is allowed only if $N \geq 3$. The configurations in (g) and (h) are coplanar states.

where α controls the phase transition temperature and $\beta_{\lambda=1,2,3}$ are interaction parameters that determine the specific ordered phase.

For general parameter values, the free energy exhibits $D_3 \times O(N) \times \mathbb{Z}_2 \times \mathbb{Z}_2$ symmetry. The D_3 symmetry corresponds to the lattice point group, while $O(N)$ represents internal rotational symmetry. The additional \mathbb{Z}_2 factors arise from the reflection symmetry of each ordering vector. This symmetry can be enhanced under specific parameter conditions: (1) When $\beta_3 = 0$, the system exhibits $D_3 \times O(N) \times O(N) \times O(N)$ symmetry, allowing independent rotations of each Δ_{Q_l} . (2) When $\beta_2 = 2\beta_1$ and $\beta_3 = 0$, the symmetry reaches its maximum $O(3N)$, treating all components of all order parameters equivalently.

For systems with $N > 3$, we can always perform an $O(N)$ rotation to restrict nonzero components to at most three dimensions, making the $N = 3$ analysis sufficient for understanding all cases with $N > 3$. Hereafter we will focus on the experimentally relevant cases of $N = 2$ (XY spins) and $N = 3$ (Heisenberg spins), which capture the essential physics of most magnetic materials on hexagonal lattices. For example, Kitaev candidate materials featuring significant trigonal distortion along with direct exchange interactions can be modeled using an easy-plane XXZ model [43, 47, 48], which is effectively represented by the $O(2)$ model in low energies.

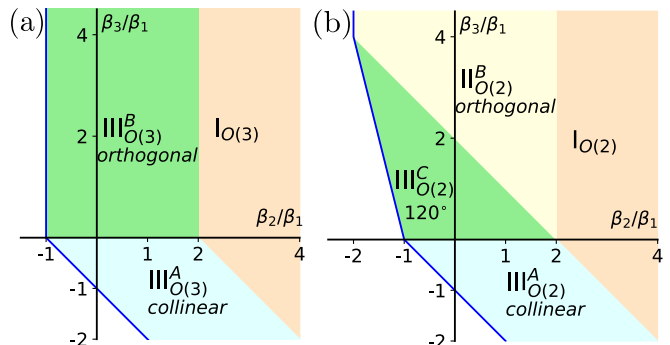


FIG. 2. Phase diagrams for (a) $O(3)$ and (b) $O(2)$ models. Notations I, II, and III denote single-, double-, and triple-Q phases, respectively. Labels A, B, and C indicate collinear, orthogonal, and 120° phases. Model (a) $O(3)$ is stable under conditions $\beta_1 > 0$, $\beta_1 + \beta_2 > 0$, and $\beta_1 + \beta_2 + \beta_3 > 0$, while model (b) $O(2)$ is stable with $\beta_1 > 0$, $2\beta_1 + \beta_2 > 0$, $\beta_1 + \beta_2 + \beta_3 > 0$, and $4(\beta_1 + \beta_2) + \beta_3 > 0$. Each phase has a unique magnetic configuration, displayed in Fig. 1(b)-(g).

Phase Diagrams — By minimizing the free energy in Eq. (1), we can identify the stable ordered phases and construct phase diagrams for the $O(N)$ model. The stability conditions require $\alpha < 0$ and $\beta_1 > 0$, with additional constraints on β_2 and β_3 specific to each phase.

$O(3)$ Model: For the $O(3)$ model relevant to Heisenberg spins, we find three distinct stable phases, as shown

in Fig. 2(a):

- **Phase I**_{*O*(3)} (Single-Q): Only one ordering vector is active, i.e., $|\Delta_{\mathbf{Q}_1}| \neq 0$ and $|\Delta_{\mathbf{Q}_2}| = |\Delta_{\mathbf{Q}_3}| = 0$.
- **Phase III**^A_{*O*(3)} (Triple-Q Collinear): All three ordering vectors $\Delta_{\mathbf{Q}_{l=1,2,3}}$ have equal amplitudes and parallel directions.
- **Phase III**^B_{*O*(3)} (Triple-Q Orthogonal): All three ordering vectors have equal amplitudes but are mutually orthogonal.

***O*(2) Model:** The *O*(2) model, applicable to XY spins, exhibits a richer phase diagram with four stable phases, as illustrated in Fig. 2(b):

- **Phase I**_{*O*(2)} (Single-Q): Similar to the *O*(3) case, only one ordering vector is present.
- **Phase II**^B_{*O*(2)} (Double-Q Orthogonal): Two ordering vectors with equal amplitudes and orthogonal directions.
- **Phase III**^A_{*O*(2)} (Triple-Q Collinear): All three ordering vectors have equal amplitudes and parallel directions.
- **Phase III**^C_{*O*(2)} (Triple-Q 120° Coplanar): All three ordering vectors have equal amplitudes with 120° angles between them in the *O*(2) plane.

Real-space Configurations — The identified phases correspond to distinct real-space magnetic configurations. For the single-Q phase, the magnetic structure forms a spin density wave along one direction. The triple-Q collinear phase represents a superposition of three spin density waves with parallel spin orientations, while the triple-Q orthogonal phase in the *O*(3) model forms a non-coplanar spin structure that can potentially host non-trivial topological properties.

Particularly interesting is the triple-Q 120° phase in the *O*(2) model, which forms a superposition of three spin density waves with 120° angles between neighboring spins. This configuration closely resembles the magnetic structure observed in materials such as Na₂Co₂TeO₆ and related compounds.

Collective Excitations — In the ordered phases, spontaneous symmetry breaking gives rise to low-energy collective modes. To analyze these excitations, we consider small fluctuations around the mean-field order parameter $\Delta_{\mathbf{Q}_i}^0$:

$$\Delta_{\mathbf{Q}_i}(\mathbf{r}, t) = \Delta_{\mathbf{Q}_i}^0 + \boldsymbol{\eta}_{\mathbf{Q}_i}(\mathbf{r}, t), \quad (2)$$

where $|\boldsymbol{\eta}_{\mathbf{Q}_i}| \ll |\Delta_{\mathbf{Q}_i}^0|$. Expanding the free energy to quadratic order in $\boldsymbol{\eta}_{\mathbf{Q}_i}$, we have

$$\begin{aligned} \mathcal{F}_{O(N)} = & \mathcal{F}_{O(N)}^0 + \alpha \sum_{l=1}^3 |\boldsymbol{\eta}_{\mathbf{Q}_l}|^2 + 2\beta_1 \sum_{l=1}^3 [2(\Delta_{\mathbf{Q}_l}^0 \cdot \boldsymbol{\eta}_{\mathbf{Q}_l})^2 + |\Delta_{\mathbf{Q}_l}^0|^2 |\boldsymbol{\eta}_{\mathbf{Q}_l}|^2] \\ & + \beta_2 \sum_{l < m} [4(\Delta_{\mathbf{Q}_l}^0 \cdot \boldsymbol{\eta}_{\mathbf{Q}_l})(\Delta_{\mathbf{Q}_m}^0 \cdot \boldsymbol{\eta}_{\mathbf{Q}_m}) + |\Delta_{\mathbf{Q}_l}^0|^2 |\boldsymbol{\eta}_{\mathbf{Q}_m}|^2 + |\Delta_{\mathbf{Q}_m}^0|^2 |\boldsymbol{\eta}_{\mathbf{Q}_l}|^2] \\ & + \beta_3 \sum_{l < m} [(\Delta_{\mathbf{Q}_l}^0 \cdot \boldsymbol{\eta}_{\mathbf{Q}_m})^2 + (\Delta_{\mathbf{Q}_m}^0 \cdot \boldsymbol{\eta}_{\mathbf{Q}_l})^2 + 2(\Delta_{\mathbf{Q}_l}^0 \cdot \boldsymbol{\eta}_{\mathbf{Q}_m})(\Delta_{\mathbf{Q}_m}^0 \cdot \boldsymbol{\eta}_{\mathbf{Q}_l}) + 2(\Delta_{\mathbf{Q}_l}^0 \cdot \Delta_{\mathbf{Q}_m}^0)(\boldsymbol{\eta}_{\mathbf{Q}_m} \cdot \boldsymbol{\eta}_{\mathbf{Q}_l})], \end{aligned} \quad (3)$$

where $\mathcal{F}_{O(N)}^0$ is the free energy of the equilibrium state. To describe the temporal and spatial evolution of these fluctuations, we construct an effective Lagrangian that preserves all the symmetries inherent to the system, namely: (i) lattice translational symmetry, (ii) internal *O*(*N*) × ℤ₂ × ℤ₂ symmetry, and (iii) *D*₃ lattice symmetry:

$$\mathcal{L}_{O(N)} = \Gamma \sum_l (\partial_t \boldsymbol{\eta}_{\mathbf{Q}_l}) \cdot (\partial_t \boldsymbol{\eta}_{\mathbf{Q}_l}) - \kappa \sum_l [(\partial_x \boldsymbol{\eta}_{\mathbf{Q}_l}) \cdot (\partial_x \boldsymbol{\eta}_{\mathbf{Q}_l}) + (\partial_y \boldsymbol{\eta}_{\mathbf{Q}_l}) \cdot (\partial_y \boldsymbol{\eta}_{\mathbf{Q}_l})] - \mathcal{F}_{O(N)}, \quad (4)$$

where Γ and κ are positive constants that represent the kinetic and spatial coupling parameters, respectively. The dynamics of the fluctuations are governed by the Euler-Lagrange equation:

$$-2\Gamma \partial_t^2 \boldsymbol{\eta}_{\mathbf{Q}_i} + 2\kappa(\partial_x^2 + \partial_y^2) \boldsymbol{\eta}_{\mathbf{Q}_i} = \frac{\partial[\delta \mathcal{F}_{O(N)}]}{\partial \boldsymbol{\eta}_{\mathbf{Q}_i}}. \quad (5)$$

For plane wave solutions of the form $\tilde{\eta}_i \propto \cos(\mathbf{q} \cdot \mathbf{r} - \omega t)$,

the energy dispersion relation becomes:

$$\omega^2 = \frac{2\kappa q^2 + \gamma_i(\alpha, \beta_1, \beta_2, \beta_3)}{2\Gamma}, \quad (6)$$

where γ_i represents a non-negative function of coefficients α and $\beta_{\lambda=1,2,3}$. This gives rise to the energy gap $\sqrt{\gamma_i/2\Gamma}$ in the long-wavelength limit ($q \rightarrow 0$).

Symmetry Breaking — The symmetry breaking pat-

terns from the initial $D_3 \times O(N) \times \mathbb{Z}_2 \times \mathbb{Z}_2$ group reveal distinct physical characteristics across different ordered phases.

For $N = 3$: (1) $I_{O(3)}$ phase breaks D_3 to C_2 and partially breaks $O(3)$, yielding residual symmetry $C_2 \times O(2)$. (2) $\text{III}_{O(3)}^A$ phase preserves D_3 while breaking internal symmetry to $O(2)$, resulting in $D_3 \times O(2)$. (3) In $\text{III}_{O(3)}^B$ phase, both D_3 and internal symmetries break, but preserves octahedral group O through combined operations.

For $N = 2$: (1) $I_{O(2)}$ phase breaks the initial symmetry to $C_2 \times \mathbb{Z}_2$. (2) In $\text{II}_{O(2)}^B$ phase, residual symmetry C_4 is generated by $C_2' \times C_4 \times (-1) \times 1$ ($\in D_3 \times O(2) \times \mathbb{Z}_2 \times \mathbb{Z}_2$). (3) In $\text{III}_{O(2)}^A$ phase, the initial symmetry breaks to $D_3 \times \mathbb{Z}_2$. (4) For $\text{III}_{O(2)}^C$ phase, combined lattice-internal operations preserve D_3 .

The spontaneous breaking of continuous symmetries results in gapless Goldstone modes [49–51]. The number of such modes equals the number of broken continuous symmetry generators. For example, in the single-Q phase of the $O(3)$ model, the reduction $O(3) \rightarrow O(2)$ produces two gapless modes with linear dispersion, $\omega(\mathbf{q}) \sim \sqrt{\kappa/\Gamma} |\mathbf{q}|$.

In contrast, amplitude (Higgs) modes [52–55] – associated with fluctuations in the magnitude of the order parameter – remain gapped. Furthermore, in multi-Q phases, such as the triple-Q 120° phase in the $O(2)$ model, the coupling between different \mathbf{Q}_l channels and the underlying D_3 lattice symmetry leads to hybridization of modes (Leggett modes [56–58]) and richer excitation spectra.

In total, the $O(N)$ model exhibits N , $2N$, and $3N$ collective modes for single-Q, double-Q, and triple-Q phases, respectively, as summarized in Table I. These gapped modes can be classified according to the residual symmetry of the corresponding ordered phase. An amplitude mode, denoted by the irreducible representation A or A_1 (refer to Table I), is consistently observed to present a universal excitation gap of $\sqrt{-2\alpha/\Gamma}$. These features can be probed by techniques such as inelastic neutron scattering [59, 60] and Raman spectroscopy [61]. It should be emphasized that considering the spin-lattice coupling will further reduce the residual symmetries and lift the degeneracy of the collective modes.

Summary and Discussion — We have developed a comprehensive Ginzburg-Landau theoretical framework for triple-Q magnetic orders on hexagonal lattices, focusing on $O(N)$ models with $N = 2$ and $N = 3$. Our key findings include: (i) Establishment of complete phase diagrams for both $N = 2$ and $N = 3$ systems, characterized by competition between interaction parameters β_1 , β_2 , and β_3 ; (ii) Identification of four distinct phases for $N = 2$ [$I_{O(2)}$, $\text{II}_{O(2)}^B$, $\text{III}_{O(2)}^A$, $\text{III}_{O(2)}^C$] and three stable phases for $N = 3$ [$I_{O(3)}$, $\text{III}_{O(3)}^A$, $\text{III}_{O(3)}^B$]; and (iii) Systematic analysis of collective excitations revealing fundamental connections between symmetry breaking patterns

TABLE I. Summary of phases, residual symmetries (Res. Symm.) of ordered phases, and collective excitations for $O(2)$ and $O(3)$ models. The collective modes are classified according to the irreducible representations of the residual symmetry group’s discrete component [45]. For the $O(3)$ model, the residual internal $O(2)$ symmetry introduces an extra two-fold degeneracy.

Model	Phase	Res. Symm.	Degeneracy	Modes
$O(2)$	$I_{O(2)}$	$C_2 \times \mathbb{Z}_2$	1 (gapped)	A
			1 (gapless)	B
	Orthogonal	C_4	1 (gapped)	A
			1 (gapped)	B
			1 (gapped)	E
			1 (gapless)	E
	Collinear	$D_3 \times \mathbb{Z}_2$	1 (gapped)	A_1
			2 (gapped)	E
			2 (gapped)	E
	$\text{III}_{O(2)}^C$ 120°	D_3	1 (gapped)	A_1
2 (gapped)			E	
2 (gapped)			E	
1 (gapless)			A_1	
$O(3)$	$I_{O(3)}$	$C_2 \times O(2)$	1 (gapped)	A
			2 (gapless)	A
	Collinear	$D_3 \times O(2)$	1 (gapped)	A_1
			2 (gapped)	E
			4 (gapped)	E
			2 (gapless)	A_1
	Orthogonal	O	1 (gapped)	A_1
			2 (gapped)	E
3 (gapped)			T_2	
			3 (gapless)	T_1

and collective modes.

These findings have significant physical implications: (i) They provide a theoretical framework for understanding complex magnetic structures observed in hexagonal lattice compounds, encompassing triangular, honeycomb, and kagome lattices; (ii) They offer specific predictions for experimental probes of magnetic excitations; and (iii) They establish a comprehensive classification system for symmetry-breaking patterns in these magnetic systems.

Future research directions include: (i) Incorporation of external fields and additional anisotropies [21, 22]; (ii) Phase transition dynamics [62]; (iii) Topological defects and excitations [63]; (iv) Extension to other internal symmetries, such as $U(N)$ models featuring complex order

parameters, is notably relevant. In particular, $U(1)$ models are intimately linked to the recently observed triple-Q pair density wave in the Kagome superconductor family AV_3Sb_5 ($A=K, Rb$ or Cs) [64–67]; and (v) Application to specific material systems with experimental validation.

Acknowledgment — We would like to thank Yuan Li and Hong Yao for their helpful discussions. This work is supported in part by the National Key Research and Development Program of China (Grant No. 2022YFA1403403), the National Natural Science Foundation of China (Grants No. 12274441 and No. 12034004). J.-T. Jin is supported by a fellowship and a CRF award from the Research Grants Council of the Hong Kong Special Administrative Region, China (Projects No. HKUST SRFS2324-6S01 and No. C7037-22GF). J.-T. Jin also acknowledge the support from the New Cornerstone Science Foundation.

* yizhou@iphy.ac.cn

- [1] V. L. Ginzburg and L. D. Landau, On the theory of superconductivity, *Zh. Eksp. Teor. Fiz.* **20**, 1064 (1950).
- [2] L. D. Landau, On the theory of phase transitions, *Zh. Eksp. Teor. Fiz.* **7**, 19 (1937).
- [3] C. D. Batista, S.-Z. Lin, S. Hayami, and Y. Kamiya, Frustration and chiral orderings in correlated electron systems, *Reports on Progress in Physics* **79**, 084504 (2016).
- [4] S. Hayami and Y. Motome, Noncoplanar multiple- Q spin textures by itinerant frustration: Effects of single-ion anisotropy and bond-dependent anisotropy, *Phys. Rev. B* **103**, 054422 (2021).
- [5] I. Martin and C. D. Batista, Itinerant electron-driven chiral magnetic ordering and spontaneous quantum hall effect in triangular lattice models, *Phys. Rev. Lett.* **101**, 156402 (2008).
- [6] Y. Kato, I. Martin, and C. D. Batista, Stability of the spontaneous quantum hall state in the triangular kondo-lattice model, *Phys. Rev. Lett.* **105**, 266405 (2010).
- [7] W. Yao, Y. Zhao, Y. Qiu, C. Balz, J. R. Stewart, J. W. Lynn, and Y. Li, Magnetic ground state of the Kitaev $Na_2Co_2TeO_6$ spin liquid candidate, *Phys. Rev. Res.* **5**, L022045 (2023).
- [8] X. Jin, M. Geng, F. Orlandi, D. Khalyavin, P. Manuel, Y. Liu, and Y. Li, Robust triple- q magnetic order with trainable spin vorticity in $Na_2Co_2TeO_6$ (2025), [arXiv:2501.07843](https://arxiv.org/abs/2501.07843).
- [9] W. G. F. Krüger, W. Chen, X. Jin, Y. Li, and L. Janssen, Triple- q Order in $Na_2Co_2TeO_6$ from Proximity to Hidden-SU(2)-Symmetric Point, *Phys. Rev. Lett.* **131**, 146702 (2023).
- [10] W. Yao, K. Iida, K. Kamazawa, and Y. Li, Excitations in the Ordered and Paramagnetic States of Honeycomb Magnet $Na_2Co_2TeO_6$, *Phys. Rev. Lett.* **129**, 147202 (2022).
- [11] A. Banerjee, J. Yan, J. Knolle, C. A. Bridges, M. B. Stone, M. D. Lumsden, D. G. Mandrus, D. A. Tennant, R. Moessner, and S. E. Nagler, Neutron scattering in the proximate quantum spin liquid $\alpha - RuCl_3$, *Science* **356**, 1055 (2017).
- [12] J. A. Sears, Y. Zhao, Z. Xu, J. W. Lynn, and Y.-J. Kim, Phase diagram of $\alpha - RuCl_3$ in an in-plane magnetic field, *Phys. Rev. B* **95**, 180411 (2017).
- [13] H. B. Cao, A. Banerjee, J.-Q. Yan, C. A. Bridges, M. D. Lumsden, D. G. Mandrus, D. A. Tennant, B. C. Chakoumakos, and S. E. Nagler, Low-temperature crystal and magnetic structure of $\alpha - RuCl_3$, *Phys. Rev. B* **93**, 134423 (2016).
- [14] H. Zhang, M. A. McGuire, A. F. May, H.-Y. Chao, Q. Zheng, M. Chi, B. C. Sales, D. G. Mandrus, S. E. Nagler, H. Miao, F. Ye, and J. Yan, Stacking disorder and thermal transport properties of $\alpha - RuCl_3$, *Phys. Rev. Mater.* **8**, 014402 (2024).
- [15] Y. Gu, X. Li, Y. Chen, K. Iida, A. Nakao, K. Munakata, V. O. Garlea, Y. Li, G. Deng, I. A. Zaliznyak, J. M. Tranquada, and Y. Li, In-plane multi- q magnetic ground state of $Na_3Co_2SbO_6$, *Phys. Rev. B* **109**, L060410 (2024).
- [16] X. Li, Y. Gu, Y. Chen, V. O. Garlea, K. Iida, K. Kamazawa, Y. Li, G. Deng, Q. Xiao, X. Zheng, Z. Ye, Y. Peng, I. A. Zaliznyak, J. M. Tranquada, and Y. Li, Giant Magnetic In-Plane Anisotropy and Competing Instabilities in $Na_3Co_2SbO_6$, *Phys. Rev. X* **12**, 041024 (2022).
- [17] P. Park, W. Cho, C. Kim, Y. An, K. Iida, R. Kajimoto, S. Matin, S.-S. Zhang, C. D. Batista, and J.-G. Park, Contrasting dynamical properties of single- q and triple- q magnetic orderings in a triangular lattice antiferromagnet, *arxiv* (2024), [arXiv:2410.02180](https://arxiv.org/abs/2410.02180).
- [18] J. A. Paddison, H. Zhang, J. Yan, M. J. Cliffe, M. A. McGuire, S.-H. Do, S. Gao, M. B. Stone, D. Dahlbom, K. Barros, *et al.*, Cubic double perovskites host noncoplanar spin textures, *npj Quantum Materials* **9**, 48 (2024).
- [19] P. Park, W. Cho, C. Kim, Y. An, Y.-G. Kang, M. Avdeev, R. Sibille, K. Iida, R. Kajimoto, K. H. Lee, *et al.*, Tetrahedral triple- q magnetic ordering and large spontaneous hall conductivity in the metallic triangular antiferromagnet $Co_{1/3}TaS_2$, *Nature Communications* **14**, 8346 (2023).
- [20] Y. Kato and Y. Motome, Magnetic field-temperature phase diagrams for multiple- Q magnetic ordering: Exact steepest descent approach to long-range interacting spin systems, *Phys. Rev. B* **105**, 174413 (2022).
- [21] L. Messio, C. Lhuillier, and G. Misguich, Lattice symmetries and regular magnetic orders in classical frustrated antiferromagnets, *Phys. Rev. B* **83**, 184401 (2011).
- [22] L. Janssen, E. C. Andrade, and M. Vojta, Honeycomb-lattice heisenberg-kitaev model in a magnetic field: Spin canting, metamagnetism, and vortex crystals, *Phys. Rev. Lett.* **117**, 277202 (2016).
- [23] W. G. F. Krüger, W. Chen, X. Jin, Y. Li, and L. Janssen, Triple- q Order in $Na_2Co_2TeO_6$ from Proximity to Hidden-SU(2)-Symmetric Point, *Phys. Rev. Lett.* **131**, 146702 (2023).
- [24] N. Francini and L. Janssen, Ferrimagnetism from triple- q order in $Na_2Co_2TeO_6$, *Phys. Rev. B* **110**, 235118 (2024).
- [25] H. Liu and G. Khaliullin, Pseudospin exchange interactions in d^7 cobalt compounds: Possible realization of the Kitaev model, *Phys. Rev. B* **97**, 014407 (2018).
- [26] R. Sano, Y. Kato, and Y. Motome, Kitaev-Heisenberg Hamiltonian for high-spin d^7 Mott insulators, *Phys. Rev. B* **97**, 014408 (2018).
- [27] H. Liu, J. Chaloupka, and G. Khaliullin, Kitaev Spin Liquid in $3d$ Transition Metal Compounds, *Phys. Rev. Lett.* **125**, 047201 (2020).
- [28] C. Kim, H.-S. Kim, and J.-G. Park, Spin-orbital entan-

- gled state and realization of Kitaev physics in 3d cobalt compounds: a progress report, *Journal of Physics: Condensed Matter* **34**, 023001 (2021).
- [29] S. Hayami, Checkerboard bubble lattice formed by octuple-period quadruple- Q spin density waves, *Phys. Rev. B* **108**, 094415 (2023).
- [30] R. Yambe and S. Hayami, Anisotropic spin model and multiple- q states in cubic systems, *Phys. Rev. B* **107**, 174408 (2023).
- [31] A. Banerjee, P. Lampen-Kelley, J. Knolle, C. Balz, A. A. Aczel, B. Winn, Y. Liu, D. Pajerowski, J. Yan, C. A. Bridges, A. T. Savici, B. C. Chakoumakos, M. D. Lumsden, D. A. Tennant, R. Moessner, D. G. Mandrus, and S. E. Nagler, Excitations in the field-induced quantum spin liquid state of α - RuCl_3 , *npj Quantum Materials* **3**, 8 (2018).
- [32] A. M. Samarakoon, Q. Chen, H. Zhou, and V. O. Garlea, Static and dynamic magnetic properties of honeycomb lattice antiferromagnets $\text{Na}_2\text{M}_2\text{TeO}_6$, $M = \text{Co}$ and Ni , *Phys. Rev. B* **104**, 184415 (2021).
- [33] X. Hong, M. Gillig, W. Yao, L. Janssen, V. Kocsis, S. Gass, Y. Li, A. U. Wolter, B. Büchner, and C. Hess, Phonon thermal transport shaped by strong spin-phonon scattering in a Kitaev material $\text{Na}_2\text{Co}_2\text{TeO}_6$, *npj Quantum Materials* **9**, 18 (2024).
- [34] P. Miao, X. Jin, W. Yao, Y. Chen, A. Koda, Z. Tan, W. Xie, W. Ji, T. Kamiyama, and Y. Li, Persistent spin dynamics in magnetically ordered honeycomb-lattice cobalt oxides, *Phys. Rev. B* **109**, 134431 (2024).
- [35] J. Wang and Z.-X. Liu, Effect of ring-exchange interactions in the extended kitaev honeycomb model, *Phys. Rev. B* **108**, 014437 (2023).
- [36] R. Pohle, N. Shannon, and Y. Motome, Eight-color chiral spin liquid in the $s = 1$ bilinear-biquadratic model with kitaev interactions, *Phys. Rev. Res.* **6**, 033077 (2024).
- [37] H. Takagi, T. Takayama, G. Jackeli, G. Khaliullin, and S. E. Nagler, Concept and realization of Kitaev quantum spin liquids, *Nat. Rev. Phys.* **1**, 264 (2019).
- [38] S. Trebst and C. Hickey, Kitaev materials, *Physics Reports* **950**, 1 (2022).
- [39] Y. Motome, R. Sano, S. Jang, Y. Sugita, and Y. Kato, Materials design of Kitaev spin liquids beyond the Jackeli–Khaliullin mechanism, *Journal of Physics: Condensed Matter* **32**, 404001 (2020).
- [40] L. Balents, Spin liquids in frustrated magnets, *Nature* **464**, 199 (2010).
- [41] Y. Zhou, K. Kanoda, and T.-K. Ng, Quantum spin liquid states, *Rev. Mod. Phys.* **89**, 025003 (2017).
- [42] C. Broholm, R. Cava, S. Kivelson, D. Nocera, M. Norman, and T. Senthil, Quantum spin liquids, *Science* **367**, eaay0668 (2020).
- [43] S. M. Winter, Magnetic couplings in edge-sharing high-spin d7 compounds, *Journal of Physics: Materials* **5**, 045003 (2022).
- [44] H. Liu, Towards Kitaev spin liquid in 3d transition metal compounds, *Int. J. Mod. Phys. B* **35**, 2130006 (2021).
- [45] G. F. Koster, J. O. Dimmock, R. G. Wheeler, and H. Statz, *The Properties of the Thirty-Two Point Groups* (The MIT Press, 1963).
- [46] M. Sigrist and K. Ueda, Phenomenological theory of unconventional superconductivity, *Rev. Mod. Phys.* **63**, 239 (1991).
- [47] S. Das, S. Voleti, T. Saha-Dasgupta, and A. Paramakanti, Xy magnetism, kitaev exchange, and long-range frustration in the $J_{\text{eff}} = \frac{1}{2}$ honeycomb cobaltates, *Phys. Rev. B* **104**, 134425 (2021).
- [48] P. A. Maksimov, A. V. Ushakov, Z. V. Pchelkina, Y. Li, S. M. Winter, and S. V. Streltsov, Ab initio guided minimal model for the “kitaev” material $\text{BaCo}_2(\text{AsO}_4)_2$: Importance of direct hopping, third-neighbor exchange, and quantum fluctuations, *Phys. Rev. B* **106**, 165131 (2022).
- [49] Y. Nambu, Quasi-particles and gauge invariance in the theory of superconductivity, *Phys. Rev.* **117**, 648 (1960).
- [50] J. Goldstone, A. Salam, and S. Weinberg, Broken symmetries, *Phys. Rev.* **127**, 965 (1962).
- [51] H. Watanabe, Counting rules of nambu–goldstone modes, *Annual Review of Condensed Matter Physics* **11**, 169 (2020).
- [52] P. W. Higgs, Broken symmetries and the masses of gauge bosons, *Phys. Rev. Lett.* **13**, 508 (1964).
- [53] P. W. Anderson, Plasmons, gauge invariance, and mass, *Phys. Rev.* **130**, 439 (1963).
- [54] D. Pekker and C. Varma, Amplitude/higgs modes in condensed matter physics, *Annual Review of Condensed Matter Physics* **6**, 269 (2015).
- [55] R. Shimano and N. Tsuji, Higgs mode in superconductors, *Annual Review of Condensed Matter Physics* **11**, 103 (2020).
- [56] A. J. Leggett, Number-phase fluctuations in two-band superconductors, *Progress of Theoretical Physics* **36**, 901 (1966).
- [57] T. Kamatani, S. Kitamura, N. Tsuji, R. Shimano, and T. Morimoto, Optical response of the leggett mode in multiband superconductors in the linear response regime, *Phys. Rev. B* **105**, 094520 (2022).
- [58] T. Yanagisawa, Nambu-goldstone-leggett modes in multicondensate superconductors, *Novel Superconducting Materials* **1**, 95 (2015).
- [59] R. S. Fishman, J. A. Fernandez-Baca, and T. Rõðm, Inelastic neutron scattering, in *Spin-Wave Theory and its Applications to Neutron Scattering and THz Spectroscopy*, 2053-2571 (Morgan & Claypool Publishers, 2018) pp. 2–1 to 2–14.
- [60] S. Klotz, M. Braden, and J. Besson, Inelastic neutron scattering to very high pressures, *Hyperfine Interactions* **128**, 245 (2000).
- [61] F. McCubbin, Raman spectroscopy, in *Encyclopedia of Astrobiology*, edited by M. Gargaud, W. M. Irvine, R. Amils, P. Claeys, H. J. Cleaves, M. Gerin, D. Rouan, T. Spohn, S. Tirard, and M. Viso (Springer Berlin Heidelberg, Berlin, Heidelberg, 2023) pp. 2619–2619.
- [62] P. C. Hohenberg and B. I. Halperin, Theory of dynamic critical phenomena, *Rev. Mod. Phys.* **49**, 435 (1977).
- [63] N. D. Mermin, The topological theory of defects in ordered media, *Rev. Mod. Phys.* **51**, 591 (1979).
- [64] H. Chen, H. Yang, B. Hu, Z. Zhao, J. Yuan, Y. Xing, G. Qian, Z. Huang, G. Li, Y. Ye, S. Ma, S. Ni, H. Zhang, Q. Yin, C. Gong, Z. Tu, H. Lei, H. Tan, S. Zhou, C. Shen, X. Dong, B. Yan, Z. Wang, and H.-J. Gao, Roton pair density wave in a strong-coupling kagome superconductor, *Nature* **599**, 222 (2021).
- [65] J.-T. Jin, K. Jiang, H. Yao, and Y. Zhou, Interplay between pair density wave and a nested fermi surface, *Phys. Rev. Lett.* **129**, 167001 (2022).
- [66] S. Zhou and Z. Wang, Chern fermi pocket, topological pair density wave, and charge-4e and charge-6e superconductivity in kagomé superconductors, *Nature Communications* **13**, 7288 (2022).

- [67] M. Yao, Y. Wang, D. Wang, J.-X. Yin, and Q.-H. Wang, Self-consistent theory of 2×2 pair density waves in kagome superconductors (2024), arXiv:2408.03056 [cond-mat.supr-con].

Supplementary Material for “Effective field theory for triple-Q magnetic orders on a hexagonal lattice”

This supplementary material elaborates further on our effective field theory. It covers the identification of each phase and presents the associated phase diagrams for $N = 2, 3$. Additionally, it details the computation of collective excitations within each phase. A concise discussion on a $U(1)$ model connected to our $O(2)$ model is also included.

I. PHASES AND PHASE DIAGRAM

In this section, we show the details on the calculation of each phase mentioned in the maintext. We begin with the minimization of the free energy $\mathcal{F}_{O(N)}$ by solving the GL equations:

$$\frac{\partial \mathcal{F}_{O(N)}}{\partial \Delta_{\mathbf{Q}_l}^p} = 0, \quad (\text{S1})$$

where $l = 1, 2, 3$. While focusing on nontrivial solutions with at least one nonzero element $|\Delta_{\mathbf{Q}_l}|$, these solutions can be classified into three categories based on the number of nonzero wave vectors \mathbf{Q}_l :

- Type I (Single-Q): Only one of the three values $|\Delta_{\mathbf{Q}_l}|$ is nonzero. Without loss of generality, we choose $|\Delta_{\mathbf{Q}_1}| \neq 0$. The corresponding free energy $\mathcal{F}_{O(N)}^I$ simplifies to:

$$\mathcal{F}_{O(N)}^I = \alpha |\Delta_{\mathbf{Q}_1}|^2 + \beta_1 |\Delta_{\mathbf{Q}_1}|^4. \quad (\text{S2})$$

- Type II (double-Q): Two of the three components $|\Delta_{\mathbf{Q}_l}|$ are nonzero. Assuming $|\Delta_{\mathbf{Q}_3}| = 0$, the free energy $\mathcal{F}_{O(N)}^{II}$ takes the form:

$$\mathcal{F}_{O(N)}^{II} = \alpha (|\Delta_{\mathbf{Q}_1}|^2 + |\Delta_{\mathbf{Q}_2}|^2) + \beta_1 (|\Delta_{\mathbf{Q}_1}|^4 + |\Delta_{\mathbf{Q}_2}|^4) + \beta_2 |\Delta_{\mathbf{Q}_1}|^2 |\Delta_{\mathbf{Q}_2}|^2 + \beta_3 (\Delta_{\mathbf{Q}_1} \cdot \Delta_{\mathbf{Q}_2})^2. \quad (\text{S3})$$

- Type III (triple-Q): All three components $|\Delta_{\mathbf{Q}_l}|$ are nonzero. The free energy $\mathcal{F}_{O(N)}^{III}$ maintains the full form as given in Eq. (1) in the maintext.

As mentioned in the maintext, the phase diagram for any $N > 3$ can be obtained directly from it for $N = 3$ due to the internal $O(N)$ symmetry. Therefore, we focus on $N = 3$ and $N = 2$ in the rest of this section. We will present the complete information of the phase diagrams shown in Fig. 2 in the maintext, including the configuration of the order parameter(s) and the corresponding free energy for each phase. Besides, some local minima obtained from Eq. (S1) may not serve as the unique global minimum for any parameter values $\{\alpha, \beta_{\lambda=1,2,3}\}$. These states (such as $II_{O(3)}^A$ and $III_{O(2)}^D$) are not included in the phase diagrams Fig. 2 but we have shown their configurations in Fig. 1.

$$N = 3$$

For single-Q states, the system exhibits a single vector $\Delta_{\mathbf{Q}_1}$ with magnitude $|\Delta_{\mathbf{Q}_1}| = \sqrt{-\alpha/2\beta_1}$ and arbitrary orientation. The corresponding free energy is $\mathcal{F}_{O(3)}^I = -\alpha^2/4\beta_1$. This solution is denoted as phase $I_{O(3)}$.

For double-Q states, we observe that

$$0 \leq (\Delta_{\mathbf{Q}_1} \cdot \Delta_{\mathbf{Q}_2})^2 \leq |\Delta_{\mathbf{Q}_1}|^2 |\Delta_{\mathbf{Q}_2}|^2,$$

where the equality holds when $\Delta_{\mathbf{Q}_1}$ and $\Delta_{\mathbf{Q}_2}$ are either orthogonal or collinear. The free energy $\mathcal{F}_{O(3)}^{II}$ reaches its minimum under different conditions depending on the sign of β_3 :

$$\begin{aligned} \text{for } \beta_3 < 0: & \quad \Delta_{\mathbf{Q}_1} \parallel \Delta_{\mathbf{Q}_2}; \\ \text{for } \beta_3 > 0: & \quad \Delta_{\mathbf{Q}_1} \cdot \Delta_{\mathbf{Q}_2} = 0. \end{aligned}$$

By solving

$$\frac{\partial \mathcal{F}_{O(3)}^{II}}{\partial |\Delta_{\mathbf{Q}_1}|} = \frac{\partial \mathcal{F}_{O(3)}^{II}}{\partial |\Delta_{\mathbf{Q}_2}|} = 0,$$

we find

$$|\Delta_{\mathbf{Q}_1}| = |\Delta_{\mathbf{Q}_2}| = \sqrt{\frac{-\alpha}{2\beta_1 + \beta_2 + \Theta(-\beta_3)\beta_3}}, \quad (\text{S4})$$

where $\Theta(x)$ is the Heaviside step function. The corresponding free energy is

$$\mathcal{F}_{O(3)}^{\text{II}} = -\frac{\alpha^2}{2\beta_1 + \beta_2 + \Theta(-\beta_3)\beta_3}. \quad (\text{S5})$$

We denote the type II state with collinear vectors as $\text{II}_{O(3)}^A$ and the state with orthogonal vectors as $\text{II}_{O(3)}^B$. For triple-Q states, we apply similar analysis using the inequalities

$$0 \leq \sum_{l < m} (\Delta_{\mathbf{Q}_l} \cdot \Delta_{\mathbf{Q}_m})^2 \leq \sum_{l < m} |\Delta_{\mathbf{Q}_l}|^2 |\Delta_{\mathbf{Q}_m}|^2.$$

When $\beta_3 < 0$, the minimum free energy corresponds to three collinear vectors (phase $\text{III}_{O(3)}^A$), while for $\beta_3 > 0$, it corresponds to three mutually orthogonal vectors (phase $\text{III}_{O(3)}^B$). Further solving

$$\frac{\partial \mathcal{F}_{O(3)}^{\text{III}}}{\partial |\Delta_{\mathbf{Q}_1}|} = \frac{\partial \mathcal{F}_{O(3)}^{\text{III}}}{\partial |\Delta_{\mathbf{Q}_2}|} = \frac{\partial \mathcal{F}_{O(3)}^{\text{III}}}{\partial |\Delta_{\mathbf{Q}_3}|} = 0,$$

gives rise to

$$|\Delta_{\mathbf{Q}_1}| = |\Delta_{\mathbf{Q}_2}| = |\Delta_{\mathbf{Q}_3}| = \sqrt{\frac{-\alpha}{2[\beta_1 + \beta_2 + \Theta(-\beta_3)\beta_3]}}, \quad (\text{S6})$$

with free energy

$$\mathcal{F}_{O(3)}^{\text{III}} = -\frac{3\alpha^2}{4[\beta_1 + \beta_2 + \Theta(-\beta_3)\beta_3]}. \quad (\text{S7})$$

The global minimum of $\mathcal{F}_{O(3)}$ must be one of these five local minima ($\text{I}_{O(3)}$, $\text{II}_{O(3)}^{A,B}$, or $\text{III}_{O(3)}^{A,B}$). The phase diagram is then obtained from the comparison of free energy among them. The result is shown in Fig. 2(a) (with their configurations in Fig. 1(b, e, f)) in the maintext. Notably, neither $\text{II}_{O(3)}^A$ nor $\text{II}_{O(3)}^B$ appears as the unique global minimum for any parameter values. System stability requires $\beta_1 > 0$, $\beta_1 + \beta_2 > 0$, and $\beta_1 + \beta_2 + \beta_3 > 0$.

$$N = 2$$

For $N = 2$, we can directly obtain the type I and type II solutions from their $N = 3$ counterparts. The solutions $\text{I}_{O(2)}$, $\text{II}_{O(2)}^A$, and $\text{II}_{O(2)}^B$ correspond directly to $\text{I}_{O(3)}$, $\text{II}_{O(3)}^A$, and $\text{II}_{O(3)}^B$. However, type III solutions require special consideration since three mutually orthogonal vectors cannot exist in two-dimensional space.

To find type III solutions for $N = 2$, we express $\Delta_{\mathbf{Q}_i}$ in polar form:

$$\Delta_{\mathbf{Q}_i} = |\Delta_{\mathbf{Q}_i}| (\cos \phi_i, \sin \phi_i)^T,$$

yielding inner products

$$\Delta_{\mathbf{Q}_i} \cdot \Delta_{\mathbf{Q}_m} = |\Delta_{\mathbf{Q}_i}| \cdot |\Delta_{\mathbf{Q}_m}| \cos(\phi_i - \phi_m).$$

The free energy in this representation becomes:

$$\mathcal{F}_{O(2)}^{\text{III}} = \alpha \sum_{l=1}^3 |\Delta_{\mathbf{Q}_l}|^2 + \beta_1 \sum_{l=1}^3 |\Delta_{\mathbf{Q}_l}|^4 + \sum_{l < m} (\beta_2 + \beta_3 \cos^2 \Phi_{lm}) |\Delta_{\mathbf{Q}_l}|^2 |\Delta_{\mathbf{Q}_m}|^2, \quad (\text{S8})$$

where $\Phi_{lm} = \phi_l - \phi_m$ represents the relative angle between vectors.

Minimizing the free energy leads to two sets of GL equations:

$$\begin{aligned} \alpha + 2\beta_1|\Delta_{\mathbf{Q}_1}|^2 + \sum_{m \neq l} (\beta_2 + \beta_3 \cos^2 \Phi_{lm}) |\Delta_{\mathbf{Q}_m}|^2 &= 0, \\ \sum_{m \neq l} |\Delta_{\mathbf{Q}_m}|^2 \sin 2\Phi_{lm} &= 0, \end{aligned} \quad (\text{S9})$$

where $l = 1, 2, 3$. While these equations yield six conditions, only five are independent. Eliminating $|\Delta_{\mathbf{Q}_l}|$ results in:

$$\sin 2\Phi_{12} = \sin 2\Phi_{23} = \sin 2\Phi_{31}. \quad (\text{S10})$$

This constraint leads to three distinct classes of solutions:

- Collinear configuration: When $\cos 2\Phi_{12} = \cos 2\Phi_{23} = \cos 2\Phi_{31} = 1$, all three vectors $\Delta_{\mathbf{Q}_i}$ are collinear. This solution, analogous to $\text{III}_{O(3)}^A$, is designated as $\text{III}_{O(2)}^A$.
- 120° configuration: When $\cos 2\Phi_{12} = \cos 2\Phi_{23} = \cos 2\Phi_{31} = -1/2$, the three vectors form a symmetric arrangement with mutual angles of 120°. This solution yields:

$$\begin{aligned} |\Delta_{\mathbf{Q}_1}| = |\Delta_{\mathbf{Q}_2}| = |\Delta_{\mathbf{Q}_3}| &= \sqrt{-\frac{2\alpha}{4(\beta_1 + \beta_2) + \beta_3}}, \\ \mathcal{F}_{O(2)}^{\text{III}} &= -\frac{3\alpha^2}{4(\beta_1 + \beta_2) + \beta_3}. \end{aligned} \quad (\text{S11})$$

We denote this coplanar solution as $\text{III}_{O(2)}^C$, illustrated in Fig. 1(g).

- Orthogonal-collinear configuration: When two values of $\cos 2\Phi_{lm}$ equal -1 and one equals 1 , two vectors align while remaining orthogonal to the third. This configuration leads to:

$$\begin{aligned} |\Delta_{\mathbf{Q}_2}| = |\Delta_{\mathbf{Q}_3}| &= \sqrt{-\frac{\alpha(2\beta_1 - \beta_2)}{4\beta_1^2 - 2\beta_2^2 + 2\beta_1(\beta_2 + \beta_3)}}, \\ |\Delta_{\mathbf{Q}_1}| &= \sqrt{-\frac{\alpha(2\beta_1 - \beta_2 + \beta_3)}{4\beta_1^2 - 2\beta_2^2 + 2\beta_1(\beta_2 + \beta_3)}}, \\ \mathcal{F}_{O(2)}^{\text{III}} &= -\frac{\alpha^2(6\beta_1 - 3\beta_2 + \beta_3)}{8\beta_1^2 - 4\beta_2^2 + 4\beta_1(\beta_2 + \beta_3)}. \end{aligned} \quad (\text{S12})$$

This solution, denoted as $\text{III}_{O(2)}^D$, appears in Fig. 1(h).

By comparing the free energies of all six candidate phases ($\text{I}_{O(2)}$, $\text{II}_{O(2)}^{A,B}$, and $\text{III}_{O(2)}^{A,C,D}$), we obtain the phase diagram shown in Fig. 2(b) (with their configurations in Fig. 1(b, d, e, g)). Notably, neither $\text{II}_{O(2)}^A$ nor $\text{III}_{O(2)}^D$ emerges as the unique global minimum for any parameter values. System stability requires three conditions: $2\beta_1 + \beta_2 > 0$, $\beta_1 + \beta_2 + \beta_3 > 0$, and $4(\beta_1 + \beta_2) + \beta_3 > 0$.

II. COLLECTIVE EXCITATIONS

In this section, we show the details on the collective excitations of the system, including the linear combinations of $\eta_{\mathbf{Q}_i}$ that give the collective modes $\tilde{\eta}_i$, and the corresponding gap-related parameters γ_i . We will give the derivation of the symmetry allowed effective Lagrangian $\mathcal{L}_{O(N)}$ at first and calculate the collective modes based on it.

Effective Lagrangian

We analyze the collective excitations through fluctuations around the equilibrium configuration based on the time-dependent GL theory. As shown in Eq. (3) in the maintext, the variation of the free energy due to the fluctuations

of order parameters can be written as

$$\begin{aligned}
\delta\mathcal{F}_{O(N)} &\equiv \mathcal{F}_{O(N)} - \mathcal{F}_{O(N)}^0 \\
&= \alpha \sum_{l=1}^3 |\boldsymbol{\eta}_{\mathbf{Q}_l}|^2 + 2\beta_1 \sum_{l=1}^3 [2(\boldsymbol{\Delta}_{\mathbf{Q}_l}^0 \cdot \boldsymbol{\eta}_{\mathbf{Q}_l})^2 + |\boldsymbol{\Delta}_{\mathbf{Q}_l}^0|^2 |\boldsymbol{\eta}_{\mathbf{Q}_l}|^2] \\
&\quad + \beta_2 \sum_{l < m} [4(\boldsymbol{\Delta}_{\mathbf{Q}_l}^0 \cdot \boldsymbol{\eta}_{\mathbf{Q}_l})(\boldsymbol{\Delta}_{\mathbf{Q}_m}^0 \cdot \boldsymbol{\eta}_{\mathbf{Q}_m}) + |\boldsymbol{\Delta}_{\mathbf{Q}_l}^0|^2 |\boldsymbol{\eta}_{\mathbf{Q}_m}|^2 + |\boldsymbol{\Delta}_{\mathbf{Q}_m}^0|^2 |\boldsymbol{\eta}_{\mathbf{Q}_l}|^2] \\
&\quad + \beta_3 \sum_{l < m} [(\boldsymbol{\Delta}_{\mathbf{Q}_l}^0 \cdot \boldsymbol{\eta}_{\mathbf{Q}_m})^2 + (\boldsymbol{\Delta}_{\mathbf{Q}_m}^0 \cdot \boldsymbol{\eta}_{\mathbf{Q}_l})^2 + 2(\boldsymbol{\Delta}_{\mathbf{Q}_l}^0 \cdot \boldsymbol{\eta}_{\mathbf{Q}_m})(\boldsymbol{\Delta}_{\mathbf{Q}_m}^0 \cdot \boldsymbol{\eta}_{\mathbf{Q}_l}) + 2(\boldsymbol{\Delta}_{\mathbf{Q}_l}^0 \cdot \boldsymbol{\Delta}_{\mathbf{Q}_m}^0)(\boldsymbol{\eta}_{\mathbf{Q}_m} \cdot \boldsymbol{\eta}_{\mathbf{Q}_l})],
\end{aligned}$$

where $\boldsymbol{\eta}_{\mathbf{Q}_l}(\mathbf{r}, t) = \boldsymbol{\Delta}_{\mathbf{Q}_l} - \boldsymbol{\Delta}_{\mathbf{Q}_l}^0$. To describe the temporal and spatial evolution of these fluctuations, we need to construct an effective Lagrangian that preserves all the symmetries inherent to the system.

In general, the effective Lagrangian $\mathcal{L}_{O(N)}$, including both temporal and spatial derivatives, is given by:

$$\begin{aligned}
\mathcal{L}_{O(N)} &= \sum_{pqlm} \Gamma_{pqlm}^1 \left(\Delta_{\mathbf{Q}_l}^p \partial_t \Delta_{\mathbf{Q}_m}^q - \Delta_{\mathbf{Q}_m}^q \partial_t \Delta_{\mathbf{Q}_l}^p \right) + \sum_{pqlm} \Gamma_{pqlm}^2 \left(\partial_t \Delta_{\mathbf{Q}_l}^p \right) \left(\partial_t \Delta_{\mathbf{Q}_m}^q \right) \\
&\quad - \sum_{\mu\nu pqlm} \kappa_{\mu\nu pqlm} \left(\partial_\mu \Delta_{\mathbf{Q}_l}^p \right) \left(\partial_\nu \Delta_{\mathbf{Q}_m}^q \right) - \mathcal{F}_{O(N)},
\end{aligned} \tag{S13}$$

where $\Gamma_{pqlm}^{1(2)}$ and $\kappa_{\mu\nu pqlm}$ are real coefficients with indices $p, q = 1, 2, \dots, N$ and $l, m = 1, 2, 3$, while $\mu, \nu = x, y$. This Lagrangian $\mathcal{L}_{O(N)}$ needs to remain invariant under the symmetry operations of the system, imposing restrictions on these constants. This symmetry includes: (i) translational symmetry, (ii) internal $O(N)$ symmetry, and (iii) D_3 rotational symmetry.

The translational symmetry requires that the total momentum of each term in $\mathcal{L}_{O(N)}$ vanishes (up to a reciprocal lattice vector), resulting in $\Gamma_{pqlm}^{1(2)} = \Gamma_{pqlm}^{1(2)} \delta_{lm}$ and $\kappa_{\mu\nu pqlm} = \kappa_{\mu\nu pql} \delta_{lm}$. In addition, the $O(N)$ symmetry allows the exchange of two components in $\boldsymbol{\Delta}_{\mathbf{Q}_l}$, i.e., $\Delta_{\mathbf{Q}_l}^p \leftrightarrow \Delta_{\mathbf{Q}_l}^q$. Thus, $\Gamma_{pql}^{1(2)}$ and $\kappa_{\mu\nu pql}$ must be symmetric under the exchange of indices p and q . However, it is easy to see that $\Delta_{\mathbf{Q}_l}^p \partial_t \Delta_{\mathbf{Q}_l}^q - \Delta_{\mathbf{Q}_l}^q \partial_t \Delta_{\mathbf{Q}_l}^p$ changes sign under the transformation $\Delta_{\mathbf{Q}_l}^p \leftrightarrow \Delta_{\mathbf{Q}_l}^q$. Thus Γ_{pql}^1 must be zero. Furthermore, the $O(N)$ symmetry also enforces that the Γ^2 and κ related terms to $O(N)$ -invariant inner products, i.e., $\sum_l \Gamma_l^2 (\partial_t \boldsymbol{\Delta}_{\mathbf{Q}_l}) \cdot (\partial_t \boldsymbol{\Delta}_{\mathbf{Q}_l})$ and $-\sum_{\mu\nu l} \kappa_{\mu\nu l} (\partial_\mu \boldsymbol{\Delta}_{\mathbf{Q}_l}) \cdot (\partial_\nu \boldsymbol{\Delta}_{\mathbf{Q}_l})$.

Then we need to consider the D_3 symmetry. Since the D_3 operations do not change the temporal derivative ∂_t , the constraint for Γ^2 related terms is simple: $\Gamma_1^2 = \Gamma_2^2 = \Gamma_3^2 \equiv \Gamma$. As for the κ related terms, there are the following 9 inequivalent terms in total,

$$\begin{aligned}
t_1 &= (\partial_x \boldsymbol{\Delta}_{\mathbf{Q}_1}) \cdot (\partial_x \boldsymbol{\Delta}_{\mathbf{Q}_1}), & t_2 &= (\partial_x \boldsymbol{\Delta}_{\mathbf{Q}_2}) \cdot (\partial_x \boldsymbol{\Delta}_{\mathbf{Q}_2}), & t_3 &= (\partial_x \boldsymbol{\Delta}_{\mathbf{Q}_3}) \cdot (\partial_x \boldsymbol{\Delta}_{\mathbf{Q}_3}), \\
t_4 &= (\partial_x \boldsymbol{\Delta}_{\mathbf{Q}_1}) \cdot (\partial_y \boldsymbol{\Delta}_{\mathbf{Q}_1}), & t_5 &= (\partial_x \boldsymbol{\Delta}_{\mathbf{Q}_2}) \cdot (\partial_y \boldsymbol{\Delta}_{\mathbf{Q}_2}), & t_6 &= (\partial_x \boldsymbol{\Delta}_{\mathbf{Q}_3}) \cdot (\partial_y \boldsymbol{\Delta}_{\mathbf{Q}_3}), \\
t_7 &= (\partial_y \boldsymbol{\Delta}_{\mathbf{Q}_1}) \cdot (\partial_y \boldsymbol{\Delta}_{\mathbf{Q}_1}), & t_8 &= (\partial_y \boldsymbol{\Delta}_{\mathbf{Q}_2}) \cdot (\partial_y \boldsymbol{\Delta}_{\mathbf{Q}_2}), & t_9 &= (\partial_y \boldsymbol{\Delta}_{\mathbf{Q}_3}) \cdot (\partial_y \boldsymbol{\Delta}_{\mathbf{Q}_3}).
\end{aligned}$$

The spatial derivative terms can be written as $\mathcal{L}_\kappa = -\sum_{i=1}^9 \kappa_i t_i$ where κ_i is the corresponding strength of t_i .

Now we apply the D_3 operators to \mathcal{L}_κ . If \mathcal{L}_κ is D_3 symmetric, all the D_3 operators keep it unchanged. This analysis will give rise to constraints on the 9 coefficients κ_i . We consider the two generators, \mathcal{A} and \mathcal{D} , of D_3 group. They act on momenta and derivatives as:

$$\begin{aligned}
\mathcal{A}(\mathbf{Q}_1, \mathbf{Q}_2, \mathbf{Q}_3) &= (\mathbf{Q}_1, \mathbf{Q}_3, \mathbf{Q}_2), \\
\mathcal{D}(\mathbf{Q}_1, \mathbf{Q}_2, \mathbf{Q}_3) &= (\mathbf{Q}_2, \mathbf{Q}_3, \mathbf{Q}_1), \\
\mathcal{A}(\partial_x, \partial_y) &= (-\partial_x, \partial_y), \\
\mathcal{D}(\partial_x, \partial_y) &= \left(\frac{1}{2} \partial_x + \frac{\sqrt{3}}{2} \partial_y, -\frac{\sqrt{3}}{2} \partial_x + \frac{1}{2} \partial_y \right).
\end{aligned}$$

It is easy to check that

$$\begin{aligned}
\mathcal{A}t_1 &= t_1, \mathcal{A}t_2 = t_3, \mathcal{A}t_3 = t_2, \\
\mathcal{A}t_4 &= -t_4, \mathcal{A}t_5 = -t_6, \mathcal{A}t_6 = -t_5, \\
\mathcal{A}t_7 &= t_7, \mathcal{A}t_8 = t_9, \mathcal{A}t_9 = t_8,
\end{aligned}$$

Thus, the condition $\mathcal{AL}_\kappa = \mathcal{L}_\kappa$ requires that $\kappa_2 = \kappa_3$, $\kappa_5 = -\kappa_6$, $\kappa_8 = \kappa_9$ and $\kappa_4 = 0$. By imposing these constraints, $\mathcal{L}_\kappa = -\kappa_1 t_1 - \kappa_2(t_2 + t_3) - \kappa_5(t_5 - t_6) - \kappa_7 t_7 - \kappa_8(t_8 + t_9)$. Then we can further apply the operator \mathcal{D} to each single term as follows,

$$\begin{aligned}\mathcal{D}t_1 &= \frac{1}{4}t_2 + \frac{3}{4}t_8 + \frac{\sqrt{3}}{4}t_5, \\ \mathcal{D}(t_2 + t_3) &= \frac{1}{4}(t_1 + t_3) + \frac{3}{4}(t_7 + t_9) + \frac{\sqrt{3}}{4}(t_4 + t_5), \\ \mathcal{D}(t_5 - t_6) &= \frac{\sqrt{3}}{4}(t_1 - t_3 - t_7 + t_9) + \frac{1}{2}(t_4 - t_6), \\ \mathcal{D}t_7 &= \frac{3}{4}t_2 + \frac{1}{4}t_8 - \frac{\sqrt{3}}{4}t_5, \\ \mathcal{D}(t_8 + t_9) &= \frac{3}{4}(t_1 + t_3) + \frac{1}{4}(t_7 + t_9) - \frac{\sqrt{3}}{4}(t_4 + t_5).\end{aligned}$$

Now the condition $\mathcal{DL}_\kappa = \mathcal{L}_\kappa$ can be expressed as

$$\begin{aligned}\kappa_1 &= \frac{1}{4}(\kappa_2 + \sqrt{3}\kappa_5 + 3\kappa_8), \\ \kappa_2 &= \frac{1}{4}(\kappa_1 + 3\kappa_7), \\ \kappa_3 = \kappa_2 &= \frac{1}{4}(\kappa_2 - \sqrt{3}\kappa_5 + 3\kappa_8), \\ \kappa_4 = 0 &= \frac{\sqrt{3}}{4}(\kappa_2 - \kappa_8) + \frac{1}{2}\kappa_5, \\ \kappa_5 &= \frac{\sqrt{3}}{4}(\kappa_1 + \kappa_2 - \kappa_7 - \kappa_8), \\ \kappa_6 = -\kappa_5 &= -\frac{1}{2}\kappa_5, \\ \kappa_7 &= \frac{1}{4}(3\kappa_2 - \sqrt{3}\kappa_5 + \kappa_8), \\ \kappa_8 &= \frac{1}{4}(3\kappa_1 + \kappa_7), \\ \kappa_9 = \kappa_8 &= \frac{1}{4}(3\kappa_2 + \sqrt{3}\kappa_5 + \kappa_8).\end{aligned}$$

The above equations give rise to $\kappa_1 = \kappa_2 = \kappa_7 = \kappa_8 \equiv \kappa$ and $\kappa_5 = 0$. Thus, \mathcal{L}_κ simplifies to

$$\mathcal{L}_\kappa = -\kappa(t_1 + t_2 + t_3 + t_7 + t_8 + t_9) = -\kappa \sum_l [(\partial_x \Delta_{\mathbf{Q}_l}) \cdot (\partial_x \Delta_{\mathbf{Q}_l}) + (\partial_y \Delta_{\mathbf{Q}_l}) \cdot (\partial_y \Delta_{\mathbf{Q}_l})].$$

Finally, the effective Lagrangian becomes

$$\begin{aligned}\mathcal{L}_{O(N)} &= \Gamma \sum_l (\partial_t \Delta_{\mathbf{Q}_l}) \cdot (\partial_t \Delta_{\mathbf{Q}_l}) - \kappa \sum_l [(\partial_x \Delta_{\mathbf{Q}_l}) \cdot (\partial_x \Delta_{\mathbf{Q}_l}) + (\partial_y \Delta_{\mathbf{Q}_l}) \cdot (\partial_y \Delta_{\mathbf{Q}_l})] - \mathcal{F}_{O(N)}, \\ &\approx \Gamma \sum_l (\partial_t \boldsymbol{\eta}_{\mathbf{Q}_l}) \cdot (\partial_t \boldsymbol{\eta}_{\mathbf{Q}_l}) - \kappa \sum_l [(\partial_x \boldsymbol{\eta}_{\mathbf{Q}_l}) \cdot (\partial_x \boldsymbol{\eta}_{\mathbf{Q}_l}) + (\partial_y \boldsymbol{\eta}_{\mathbf{Q}_l}) \cdot (\partial_y \boldsymbol{\eta}_{\mathbf{Q}_l})] - \mathcal{F}_{O(N)},\end{aligned}\tag{S14}$$

where Γ and κ are positive constants that represent the kinetic and spatial coupling parameters, respectively. This is exact Eq. (4) in the maintext.

The dynamics of the fluctuations are governed by the Euler-Lagrange equation, which is given as follows:

$$\partial_t \left(\frac{\partial \mathcal{L}_{O(N)}}{\partial (\partial_t \boldsymbol{\eta}_{\mathbf{Q}_l})} \right) + \partial_x \left(\frac{\partial \mathcal{L}_{O(N)}}{\partial (\partial_x \boldsymbol{\eta}_{\mathbf{Q}_l})} \right) + \partial_y \left(\frac{\partial \mathcal{L}_{O(N)}}{\partial (\partial_y \boldsymbol{\eta}_{\mathbf{Q}_l})} \right) = \frac{\partial \mathcal{L}_{O(N)}}{\partial \boldsymbol{\eta}_{\mathbf{Q}_l}} = -\frac{\partial [\delta \mathcal{F}_{O(N)}]}{\partial \boldsymbol{\eta}_{\mathbf{Q}_l}}.\tag{S15}$$

It gives rise to the equation of motion Eq. (5) in the maintext.

In the remainder of this section, we analyze the collective excitations for different phases based on Eq. (5) in the maintext. For convenience, we introduce the differential operator

$$\square \equiv -2\Gamma \partial_t^2 + 2\kappa(\partial_x^2 + \partial_y^2)$$

and set $|\Delta_{\mathbf{Q}_l}^0| \equiv \Delta$ for all nonzero order parameters. We want to obtain γ_i in Eq. (6) in the maintext for each $\tilde{\eta}_i$.

Collective excitations for $N = 2$

We explore the collective excitations for the $N = 2$ scenario by studying each phase sequentially from the simplest to the most complex. For every instance, the fluctuations around the equilibrium state result in both gapped and gapless modes, whose characteristics are closely associated with symmetry breaking.

Phase I_{O(2)}: In the simplest case, the equilibrium is characterized by a single order parameter. We set

$$\Delta_{\mathbf{Q}_1}^0 = \Delta (1, 0)^T,$$

where $\Delta = \sqrt{-\alpha/2\beta_1}$, and decompose the fluctuation as

$$\boldsymbol{\eta}_{\mathbf{Q}_1} = (\eta_{\mathbf{Q}_1}^1, \eta_{\mathbf{Q}_1}^2)^T.$$

This leads to two decoupled differential equations:

$$\square \eta_{\mathbf{Q}_1}^1 = -4\alpha \eta_{\mathbf{Q}_1}^1, \quad (\text{S16a})$$

$$\square \eta_{\mathbf{Q}_1}^2 = 0. \quad (\text{S16b})$$

In this context, the modes

$$\tilde{\eta}_1 = \eta_{\mathbf{Q}_1}^1 \quad \text{and} \quad \tilde{\eta}_2 = \eta_{\mathbf{Q}_1}^2$$

demonstrate a gapped excitation with a gap of $\gamma_1 = -4\alpha$ and a gapless excitation characterized by $\gamma_2 = 0$, respectively. The presence of the gapless mode indicates the occurrence of a Goldstone mode due to the breaking of the internal $O(2)$ symmetry.

Phase II_{O(2)}^B: Subsequently, we analyze a phase characterized by the presence of two orthogonal order parameters. We utilize

$$\Delta_{\mathbf{Q}_1}^0 = \Delta (1, 0)^T \quad \text{and} \quad \Delta_{\mathbf{Q}_2}^0 = \Delta (0, 1)^T,$$

with $\Delta = \sqrt{\frac{-\alpha}{2\beta_1 + \beta_2}}$, to represent this scenario and describe the fluctuations as

$$\boldsymbol{\eta}_{\mathbf{Q}_l} = (\eta_{\mathbf{Q}_l}^1, \eta_{\mathbf{Q}_l}^2)^T, \quad (l = 1, 2).$$

The resulting equations of motion read:

$$\square \begin{pmatrix} \eta_{\mathbf{Q}_1}^1 \\ \eta_{\mathbf{Q}_1}^2 \\ \eta_{\mathbf{Q}_2}^1 \\ \eta_{\mathbf{Q}_2}^2 \end{pmatrix} = 2\Delta^2 \begin{pmatrix} 4\beta_1 & 0 & 0 & 2\beta_2 \\ 0 & \beta_3 & \beta_3 & 0 \\ 0 & \beta_3 & \beta_3 & 0 \\ 2\beta_2 & 0 & 0 & 4\beta_1 \end{pmatrix} \begin{pmatrix} \eta_{\mathbf{Q}_1}^1 \\ \eta_{\mathbf{Q}_1}^2 \\ \eta_{\mathbf{Q}_2}^1 \\ \eta_{\mathbf{Q}_2}^2 \end{pmatrix} \quad (\text{S17})$$

Straightforward algebra reveals that the four collective modes can be described as

$$\tilde{\eta}_{1,2} = \eta_{\mathbf{Q}_1}^1 \pm \eta_{\mathbf{Q}_2}^2 \quad \text{and} \quad \tilde{\eta}_{3,4} = \eta_{\mathbf{Q}_1}^2 \pm \eta_{\mathbf{Q}_2}^1,$$

with the following gaps:

$$\gamma_1 = -4\alpha, \quad \gamma_2 = 4(2\beta_1 - \beta_2)\Delta^2, \quad \gamma_3 = 4\beta_3\Delta^2, \quad \gamma_4 = 0.$$

Once more, the appearance of the gapless mode is due to the broken $O(2)$ symmetry.

Phase III_{O(2)}^A: For a phase with three parallel order parameters, we choose

$$\Delta_{\mathbf{Q}_l}^0 = \Delta (1, 0)^T, \quad l = 1, 2, 3,$$

where $\Delta = \sqrt{\frac{-\alpha}{2[\beta_1 + \beta_2 + \beta_3]}}$, and write the fluctuations as

$$\boldsymbol{\eta}_{\mathbf{Q}_l} = (\eta_{\mathbf{Q}_l}^1, \eta_{\mathbf{Q}_l}^2)^T.$$

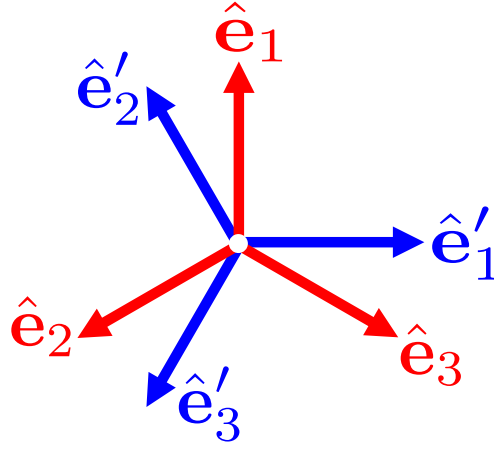


FIG. S1. Unit vectors that form the basis for the decomposition of $\Delta_{\mathbf{Q}_l}$ and $\eta_{\mathbf{Q}_l}$ for phase $\text{III}_{O(2)}^C$.

The equations of motion then separate into two independent sets:

$$\square \begin{pmatrix} \eta_{\mathbf{Q}_1}^1 \\ \eta_{\mathbf{Q}_2}^1 \\ \eta_{\mathbf{Q}_3}^1 \end{pmatrix} = 4\Delta^2 \begin{pmatrix} 2\beta_1 & \beta_2 + \beta_3 & \beta_2 + \beta_3 \\ \beta_2 + \beta_3 & 2\beta_1 & \beta_2 + \beta_3 \\ \beta_2 + \beta_3 & \beta_2 + \beta_3 & 2\beta_1 \end{pmatrix} \begin{pmatrix} \eta_{\mathbf{Q}_1}^1 \\ \eta_{\mathbf{Q}_2}^1 \\ \eta_{\mathbf{Q}_3}^1 \end{pmatrix}, \quad (\text{S18a})$$

$$\square \begin{pmatrix} \eta_{\mathbf{Q}_1}^2 \\ \eta_{\mathbf{Q}_2}^2 \\ \eta_{\mathbf{Q}_3}^2 \end{pmatrix} = 2\beta_3\Delta^2 \begin{pmatrix} -2 & 1 & 1 \\ 1 & -2 & 1 \\ 1 & 1 & -2 \end{pmatrix} \begin{pmatrix} \eta_{\mathbf{Q}_1}^2 \\ \eta_{\mathbf{Q}_2}^2 \\ \eta_{\mathbf{Q}_3}^2 \end{pmatrix}. \quad (\text{S18b})$$

The linear combination defined as

$$\tilde{\eta}_1 = \eta_{\mathbf{Q}_1}^1 + \eta_{\mathbf{Q}_2}^1 + \eta_{\mathbf{Q}_3}^1$$

is associated with a gapped mode characterized by a gap $\gamma_1 = -4\alpha$. The other two linear combinations involving the $\eta_{\mathbf{Q}_l}^1$ result in degenerate gapped modes with

$$\gamma_2 = \gamma_3 = 4(2\beta_1 - \beta_2 - \beta_3)\Delta^2.$$

In parallel, a gapless mode is produced in the $\eta_{\mathbf{Q}_l}^2$ domain, expressed as:

$$\tilde{\eta}_6 = \eta_{\mathbf{Q}_1}^2 + \eta_{\mathbf{Q}_2}^2 + \eta_{\mathbf{Q}_3}^2 \quad (\gamma_6 = 0),$$

while the two other independent combinations result in degenerate gapped modes given by

$$\gamma_4 = \gamma_5 = -6\beta_3\Delta^2.$$

Phase $\text{III}_{O(2)}^C$: In the phase characterized by the most intricate structure, where rotation of the order parameters occurs, each of the three parameters points in unique directions. Namely, we have

$$\Delta_{\mathbf{Q}_l}^0 = \Delta \hat{e}_l,$$

where $\Delta = \sqrt{-\frac{2\alpha}{4(\beta_1 + \beta_2) + \beta_3}}$, and the unit vectors are specified as follows:

$$\hat{e}_1 = (0, 1)^T, \quad \hat{e}_2 = \left(-\frac{\sqrt{3}}{2}, -\frac{1}{2}\right)^T, \quad \hat{e}_3 = \left(\frac{\sqrt{3}}{2}, -\frac{1}{2}\right)^T.$$

It is useful to define perpendicular unit vectors in addition:

$$\hat{e}'_1 = (1, 0)^T, \quad \hat{e}'_2 = \left(-\frac{1}{2}, \frac{\sqrt{3}}{2}\right)^T, \quad \hat{e}'_3 = \left(-\frac{1}{2}, -\frac{\sqrt{3}}{2}\right)^T.$$

These vectors satisfy the orthogonality requirement $\hat{e}_l \cdot \hat{e}'_l = 0$. For $l \neq m$, we also have

$$\hat{e}_l \cdot \hat{e}_m = \hat{e}'_l \cdot \hat{e}'_m = -\frac{1}{2} \quad \text{and} \quad \hat{e}_l \cdot \hat{e}'_m = \frac{\sqrt{3}}{2} \epsilon_{lm},$$

where ϵ_{lm} denotes the antisymmetric tensor. When the fluctuation field is expanded on this basis:

$$\boldsymbol{\eta}_{\mathbf{Q}_l} = \eta_{\mathbf{Q}_l}^1 \hat{e}_l + \eta_{\mathbf{Q}_l}^2 \hat{e}'_l,$$

it allows the derivative terms in the free energy to decouple along these specified directions.

Furthermore, the equilibrium and fluctuation fields yield the following relations:

$$\begin{aligned} \Delta_{\mathbf{Q}_l}^0 \cdot \Delta_{\mathbf{Q}_m}^0 &= -\frac{1}{2} \Delta^2 \quad (l \neq m), \\ \Delta_{\mathbf{Q}_l}^0 \cdot \boldsymbol{\eta}_{\mathbf{Q}_l} &= \Delta \eta_{\mathbf{Q}_l}^1, \\ \Delta_{\mathbf{Q}_l}^0 \cdot \boldsymbol{\eta}_{\mathbf{Q}_m} + \Delta_{\mathbf{Q}_m}^0 \cdot \boldsymbol{\eta}_{\mathbf{Q}_l} &= -\frac{1}{2} \Delta (\eta_{\mathbf{Q}_l}^1 + \eta_{\mathbf{Q}_m}^1) - \frac{\sqrt{3}}{2} \Delta \epsilon_{lm} (\eta_{\mathbf{Q}_l}^2 - \eta_{\mathbf{Q}_m}^2). \end{aligned}$$

The equations of motion for the six fluctuation components can then be jointly written as

$$\square \begin{pmatrix} \eta_{\mathbf{Q}_1}^1 \\ \eta_{\mathbf{Q}_2}^1 \\ \eta_{\mathbf{Q}_3}^1 \\ \eta_{\mathbf{Q}_1}^2 \\ \eta_{\mathbf{Q}_2}^2 \\ \eta_{\mathbf{Q}_3}^2 \end{pmatrix} = \Delta^2 \begin{pmatrix} 8\beta_1 & 4\beta_2 + \beta_3 & 4\beta_2 + \beta_3 & 0 & -\sqrt{3}\beta_3 & \sqrt{3}\beta_3 \\ 4\beta_2 + \beta_3 & 8\beta_1 & 4\beta_2 + \beta_3 & \sqrt{3}\beta_3 & 0 & -\sqrt{3}\beta_3 \\ 4\beta_2 + \beta_3 & 4\beta_2 + \beta_3 & 8\beta_1 & -\sqrt{3}\beta_3 & \sqrt{3}\beta_3 & 0 \\ 0 & \sqrt{3}\beta_3 & -\sqrt{3}\beta_3 & 2\beta_3 & -\beta_3 & -\beta_3 \\ -\sqrt{3}\beta_3 & 0 & \sqrt{3}\beta_3 & -\beta_3 & 2\beta_3 & -\beta_3 \\ \sqrt{3}\beta_3 & -\sqrt{3}\beta_3 & 0 & -\beta_3 & -\beta_3 & 2\beta_3 \end{pmatrix} \begin{pmatrix} \eta_{\mathbf{Q}_1}^1 \\ \eta_{\mathbf{Q}_2}^1 \\ \eta_{\mathbf{Q}_3}^1 \\ \eta_{\mathbf{Q}_1}^2 \\ \eta_{\mathbf{Q}_2}^2 \\ \eta_{\mathbf{Q}_3}^2 \end{pmatrix}. \quad (\text{S19})$$

A mode analysis reveals that among the six collective modes, two can be directly identified:

- The gapped mode

$$\tilde{\eta}_1 = \eta_{\mathbf{Q}_1}^1 + \eta_{\mathbf{Q}_2}^1 + \eta_{\mathbf{Q}_3}^1, \quad \gamma_1 = -4\alpha,$$

- The gapless (Goldstone) mode

$$\tilde{\eta}_2 = \eta_{\mathbf{Q}_1}^2 + \eta_{\mathbf{Q}_2}^2 + \eta_{\mathbf{Q}_3}^2, \quad \gamma_2 = 0.$$

The four remaining modes involve mixing between the $\eta_{\mathbf{Q}_l}^1$ and $\eta_{\mathbf{Q}_l}^2$ sectors and appear as two degenerate pairs. They can be written as:

$$\begin{aligned} \tilde{\eta}_3 &= \frac{1}{\beta_1} \left[(\gamma_3/\Delta^2 - 3\beta_3) (\eta_{\mathbf{Q}_1}^1 + \eta_{\mathbf{Q}_2}^1 - 2\eta_{\mathbf{Q}_3}^1) + 3\sqrt{3}\beta_3 (\eta_{\mathbf{Q}_1}^2 - \eta_{\mathbf{Q}_2}^2) \right], \\ \tilde{\eta}_4 &= \frac{1}{\beta_1} \left[(\gamma_4/\Delta^2 - 3\beta_3) (\eta_{\mathbf{Q}_1}^1 - 2\eta_{\mathbf{Q}_2}^1 + \eta_{\mathbf{Q}_3}^1) - 3\sqrt{3}\beta_3 (\eta_{\mathbf{Q}_1}^2 - \eta_{\mathbf{Q}_3}^2) \right], \\ \tilde{\eta}_5 &= \frac{1}{\beta_1} \left[(\gamma_5/\Delta^2 - 3\beta_3) (\eta_{\mathbf{Q}_1}^1 + \eta_{\mathbf{Q}_2}^1 - 2\eta_{\mathbf{Q}_3}^1) + 3\sqrt{3}\beta_3 (\eta_{\mathbf{Q}_1}^2 - \eta_{\mathbf{Q}_2}^2) \right], \\ \tilde{\eta}_6 &= \frac{1}{\beta_1} \left[(\gamma_6/\Delta^2 - 3\beta_3) (\eta_{\mathbf{Q}_1}^1 - 2\eta_{\mathbf{Q}_2}^1 + \eta_{\mathbf{Q}_3}^1) - 3\sqrt{3}\beta_3 (\eta_{\mathbf{Q}_1}^2 - \eta_{\mathbf{Q}_3}^2) \right], \end{aligned}$$

with the eigenvalues given by

$$\gamma_3 = \gamma_4 = \Delta^2 \left[2(2\beta_1 - \beta_2) + \beta_3 - \sqrt{4(2\beta_1 - \beta_2)^2 - 8(2\beta_1 - \beta_2)\beta_3 + 13\beta_3^2} \right], \quad (\text{S20a})$$

$$\gamma_5 = \gamma_6 = \Delta^2 \left[2(2\beta_1 - \beta_2) + \beta_3 + \sqrt{4(2\beta_1 - \beta_2)^2 - 8(2\beta_1 - \beta_2)\beta_3 + 13\beta_3^2} \right]. \quad (\text{S20b})$$

Collective excitations for $N = 3$

We proceed by extending our analysis to systems with $N = 3$, using the understanding gained from the $N = 2$ scenario as our basis. With a focus on the influence of the extra degree of freedom on the collective modes, we delve into each phase with growing complexity.

Phase $I_{O(3)}$: In the simplest phase involving only one order parameter, we define

$$\Delta_{\mathbf{Q}_1}^0 = (1, 0, 0)^T$$

where $\Delta = \sqrt{-\alpha/2\beta_1}$, and represent the fluctuation field by

$$\boldsymbol{\eta}_{\mathbf{Q}_1} = (\eta_{\mathbf{Q}_1}^1, \eta_{\mathbf{Q}_1}^2, \eta_{\mathbf{Q}_1}^3)^T.$$

The equations of motion become fully decoupled:

$$\square \eta_{\mathbf{Q}_1}^1 = -4\alpha \eta_{\mathbf{Q}_1}^1, \quad (\text{S21a})$$

$$\square \eta_{\mathbf{Q}_1}^2 = 0, \quad (\text{S21b})$$

$$\square \eta_{\mathbf{Q}_1}^3 = 0. \quad (\text{S21c})$$

The collective modes correspond directly to the components: $\tilde{\eta}_i = \eta_{\mathbf{Q}_1}^{p=i}$ ($i = 1, 2, 3$), where $\tilde{\eta}_1$ is gapped with $\gamma_1 = -4\alpha$, while the modes $\tilde{\eta}_2$ and $\tilde{\eta}_3$ are gapless with $\gamma_2 = \gamma_3 = 0$. The two gapless modes reflect the spontaneous breaking of the $O(3)$ symmetry to $O(2)$.

Phase $\text{III}_{O(3)}^A$: In the phase characterized by three parallel order parameters, we set

$$\Delta_{\mathbf{Q}_l}^0 = \Delta(1, 0, 0)^T, \quad l = 1, 2, 3,$$

accompanied by fluctuations given by

$$\boldsymbol{\eta}_{\mathbf{Q}_l} = (\eta_{\mathbf{Q}_l}^1, \eta_{\mathbf{Q}_l}^2, \eta_{\mathbf{Q}_l}^3)^T,$$

where $\Delta = \sqrt{\frac{-\alpha}{2[\beta_1 + \beta_2 + \beta_3]}}$. The expressions for $\eta_{\mathbf{Q}_l}^1$ and $\eta_{\mathbf{Q}_l}^2$ correspond directly to phase $\text{III}_{O(2)}^A$, resulting in six collective modes ($\tilde{\eta}_1$ through $\tilde{\eta}_6$). Similarly, the expressions for $\eta_{\mathbf{Q}_l}^3$ are identical to those for $\eta_{\mathbf{Q}_l}^2$, which is attributable to the $O(2)$ symmetry present in the plane orthogonal to $\Delta_{\mathbf{Q}_l}^0$. This yields three additional modes:

- Two degenerate gapped modes:

$$\tilde{\eta}_7 = \eta_{\mathbf{Q}_1}^3 - \eta_{\mathbf{Q}_2}^3, \quad \tilde{\eta}_8 = \eta_{\mathbf{Q}_1}^3 - \eta_{\mathbf{Q}_3}^3$$

with $\gamma_7 = \gamma_8 = -6\beta_3\Delta^2$;

- One gapless mode:

$$\tilde{\eta}_9 = \eta_{\mathbf{Q}_1}^3 + \eta_{\mathbf{Q}_2}^3 + \eta_{\mathbf{Q}_3}^3$$

with $\gamma_9 = 0$.

In total, this phase exhibits seven gapped modes and two gapless modes.

Phase $\text{III}_{O(3)}^B$: In the most complex configuration, the three order parameters are mutually perpendicular:

$$\Delta_{\mathbf{Q}_1}^0 = \Delta(1, 0, 0)^T, \quad \Delta_{\mathbf{Q}_2}^0 = \Delta(0, 1, 0)^T, \quad \Delta_{\mathbf{Q}_3}^0 = \Delta(0, 0, 1)^T,$$

with fluctuations $\boldsymbol{\eta}_{\mathbf{Q}_l} = (\eta_{\mathbf{Q}_l}^1, \eta_{\mathbf{Q}_l}^2, \eta_{\mathbf{Q}_l}^3)^T$, where $\Delta = \sqrt{\frac{-\alpha}{2(\beta_1 + \beta_2)}}$.

This configuration yields $\Delta_{\mathbf{Q}_l}^0 \cdot \boldsymbol{\eta}_{\mathbf{Q}_m} = \Delta \eta_{\mathbf{Q}_m}^l$. The nine components $\eta_{\mathbf{Q}_l}^p$ separate into four coupled sets:

$$\square \begin{pmatrix} \eta_{\mathbf{Q}_1}^1 \\ \eta_{\mathbf{Q}_2}^2 \\ \eta_{\mathbf{Q}_3}^3 \end{pmatrix} = 4\Delta^2 \begin{pmatrix} 2\beta_1 & \beta_2 + \beta_3 & \beta_2 \\ \beta_2 & 2\beta_1 & \beta_2 \\ \beta_2 & \beta_2 & 2\beta_1 \end{pmatrix} \begin{pmatrix} \eta_{\mathbf{Q}_1}^1 \\ \eta_{\mathbf{Q}_2}^2 \\ \eta_{\mathbf{Q}_3}^3 \end{pmatrix}, \quad (\text{S22a})$$

$$\square \begin{pmatrix} \eta_{\mathbf{Q}_1}^2 \\ \eta_{\mathbf{Q}_2}^1 \end{pmatrix} = 2\beta_3\Delta^2 \begin{pmatrix} 1 & 1 \\ 1 & 1 \end{pmatrix} \begin{pmatrix} \eta_{\mathbf{Q}_1}^2 \\ \eta_{\mathbf{Q}_2}^1 \end{pmatrix}, \quad (\text{S22b})$$

$$\square \begin{pmatrix} \eta_{\mathbf{Q}_1}^3 \\ \eta_{\mathbf{Q}_3}^1 \end{pmatrix} = 2\beta_3\Delta^2 \begin{pmatrix} 1 & 1 \\ 1 & 1 \end{pmatrix} \begin{pmatrix} \eta_{\mathbf{Q}_1}^3 \\ \eta_{\mathbf{Q}_3}^1 \end{pmatrix}, \quad (\text{S22c})$$

$$\square \begin{pmatrix} \eta_{\mathbf{Q}_2}^3 \\ \eta_{\mathbf{Q}_3}^2 \end{pmatrix} = 2\beta_3\Delta^2 \begin{pmatrix} 1 & 1 \\ 1 & 1 \end{pmatrix} \begin{pmatrix} \eta_{\mathbf{Q}_2}^3 \\ \eta_{\mathbf{Q}_3}^2 \end{pmatrix}. \quad (\text{S22d})$$

Analysis of these coupled equations of motion leads to nine collective modes:

- One gapped mode with $\gamma_1 = -4\alpha$:

$$\tilde{\eta}_1 = \eta_{\mathbf{Q}_1}^1 + \eta_{\mathbf{Q}_2}^2 + \eta_{\mathbf{Q}_3}^3.$$

- Two degenerate gapped modes with $\gamma_2 = \gamma_3 = 4(2\beta_1 - \beta_2)\Delta^2$:

$$\tilde{\eta}_2 = \eta_{\mathbf{Q}_1}^1 - \eta_{\mathbf{Q}_2}^2, \quad \tilde{\eta}_3 = \eta_{\mathbf{Q}_1}^1 - \eta_{\mathbf{Q}_3}^3.$$

- Three degenerate gapped modes with $\gamma_4 = \gamma_5 = \gamma_6 = 4\beta_3\Delta^2$:

$$\tilde{\eta}_4 = \eta_{\mathbf{Q}_1}^2 + \eta_{\mathbf{Q}_2}^1, \quad \tilde{\eta}_5 = \eta_{\mathbf{Q}_1}^3 + \eta_{\mathbf{Q}_3}^1, \quad \tilde{\eta}_6 = \eta_{\mathbf{Q}_2}^3 + \eta_{\mathbf{Q}_3}^2.$$

- Three degenerate gapless modes with $\gamma_7 = \gamma_8 = \gamma_9 = 0$:

$$\tilde{\eta}_7 = \eta_{\mathbf{Q}_1}^2 - \eta_{\mathbf{Q}_2}^1, \quad \tilde{\eta}_8 = \eta_{\mathbf{Q}_1}^3 - \eta_{\mathbf{Q}_3}^1, \quad \tilde{\eta}_9 = \eta_{\mathbf{Q}_2}^3 - \eta_{\mathbf{Q}_3}^2.$$

III. U(1) MODEL

The results for $N = 2$ can help us study certain systems described by three complex scalar order parameters $\Delta_{\mathbf{Q}_l}$ ($l = 1, 2, 3$) on hexagonal lattice. We give a brief discussion on this point in this section.

In addition to D_3 rotational symmetry and lattice translational symmetry, we consider a U(1) symmetric theory. Here the U(1) symmetry means that for any transformation $\Delta_{\mathbf{Q}_l} \mapsto \Delta_{\mathbf{Q}_l} e^{i\theta}$, the free energy $\mathcal{F}_{U(1)}$ of the system unchanged, where θ is a real number. For such a system, $\mathcal{F}_{U(1)}$ is of the following form,

$$\mathcal{F}_{U(1)} = \alpha^{U(1)} \sum_{l=1}^3 |\Delta_{\mathbf{Q}_l}|^2 + \beta_1^{U(1)} \sum_{l=1}^3 |\Delta_{\mathbf{Q}_l}|^4 + \beta_2^{U(1)} \sum_{l<m} |\Delta_{\mathbf{Q}_l}|^2 |\Delta_{\mathbf{Q}_m}|^2 + \beta_3^{U(1)} \sum_{l<m} (\Delta_{\mathbf{Q}_l} \Delta_{\mathbf{Q}_m}^*)^2 + c.c.. \quad (\text{S23})$$

We can use two values $|\Delta_{\mathbf{Q}_l}|$ and θ_l to define each $\Delta_{\mathbf{Q}_l}$, i.e., $\Delta_{\mathbf{Q}_l} = |\Delta_{\mathbf{Q}_l}| e^{i\theta_l}$. Then the $\beta_3^{U(1)}$ related terms in Eq. (S23) can be expressed as

$$\beta_3^{U(1)} \sum_{l<m} (\Delta_{\mathbf{Q}_l} \Delta_{\mathbf{Q}_m}^*)^2 + c.c. = 2\beta_3^{U(1)} \sum_{l<m} |\Delta_{\mathbf{Q}_l}|^2 |\Delta_{\mathbf{Q}_m}|^2 \cos(2\theta_l - 2\theta_m). \quad (\text{S24})$$

By comparing $\mathcal{F}_{U(1)}$ with $\mathcal{F}_{O(2)}$, we can obtain the properties of $\mathcal{F}_{U(1)}$ through the following mapping,

$$\begin{aligned} |\Delta_{\mathbf{Q}_l}| &\mapsto |\Delta_{\mathbf{Q}_l}|, & \phi_l &\mapsto \theta_l, \\ \alpha &\mapsto \alpha^{U(1)}, & \beta_1 &\mapsto \beta_1^{U(1)}, \\ \beta_2 + \frac{\beta_3}{2} &\mapsto \beta_2^{U(1)}, & \frac{\beta_3}{4} &\mapsto \beta_3^{U(1)}. \end{aligned}$$

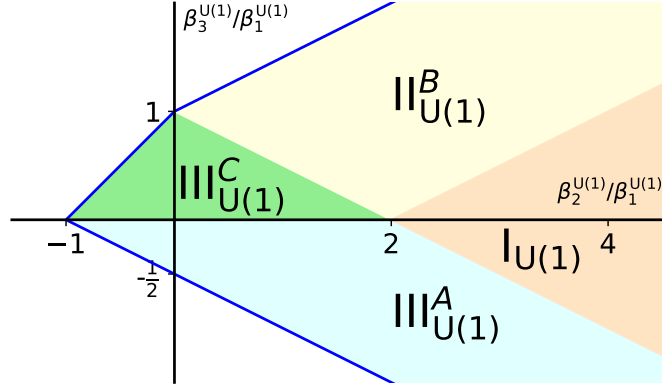


FIG. S2. The phase diagram and the stable region for $\mathcal{F}_{U(1)}$.

From this mapping, we can obtain the phase diagram of $\mathcal{F}_{U(1)}$. The result is shown in Fig. S2. The phases $I_{O(2)}$, $\Pi_{O(2)}^B$ and $\text{III}_{O(2)}^{A(C)}$ are mapped to $I_{U(1)}$, $\Pi_{U(1)}^B$ and $\text{III}_{U(1)}^{A(C)}$, respectively. The same mapping will also give rise to the stable conditions: $\beta_2^{U(1)} - 2\beta_3^{U(1)} + 2\beta_1^{U(1)} > 0$, $\beta_2^{U(1)} + 2\beta_3^{U(1)} + \beta_1^{U(1)} > 0$ and $\beta_2^{U(1)} - \beta_3^{U(1)} + \beta_1^{U(1)} > 0$, along with the conditions $\alpha^{U(1)} < 0$ and $\beta_1^{U(1)} > 0$.